ISSN 1674-1056
http://cpb.iphy.ac.cn
http://iopscience.iop.org/cpb
中国物理 B
Chinese Physics
中国物理 Chinese Physics B

Effect of chemical ordering annealing on superelasticity of Ni-Mn-Ga-Fe ferromagnetic shape memory alloy microwires

Yanfen Liu(刘艳芬), Xuexi Zhang(张学习), Hongxian Shen(沈红先), Jianfei Sun(孙剑飞), Qinan Li(李奇楠), Xiaohua Liu(刘晓华), Jianjun Li(李建军), Weidong Cheng(程伟东)
Citation: Chin. Phys. B . 2020, 29(5): 056202 . **doi:** 10.1088/1674-1056/ab8213
Journal homepage: http://cpb.iphy.ac.cn; http://iopscience.iop.org/cpb

What follows is a list of articles you may be interested in

Effect of P impurity on mechanical properties of NiAlΣ5 grain boundary: From perspectives of stress and energy

Xue-Lan Hu(胡雪兰), Ruo-Xi Zhao(赵若汐), Jiang-Ge Deng(邓江革), Yan-Min Hu(胡艳敏), Qing-Gong Song(宋庆功)
Chin. Phys. B . 2018, 27(3): 037105 . **doi:** 10.1088/1674-1056/27/3/037105

First-principles studies of effects of interstitial boron and carbon on the structural, elastic, and electronic properties of Ni solution and Ni_3Al intermetallics

Meng-Li Huang(黄梦礼), Chong-Yu Wang(王崇愚)
Chin. Phys. B . 2016, 25(10): 107104 . **doi:** 10.1088/1674-1056/25/10/107104

Electronic structures and magnetisms of the $Co_2TiSb_{1-x}Sn_x$ (x=0, 0.25, 0.5) Heusler alloys: A theoretical study of the shape-memory behavior

Wang Li-Ying, Dai Xue-Fang, Wang Xiao-Tian, Lin Ting-Ting, Chen Lei, Liu Ran, Cui Yu-Ting, Liu Guo-Dong
Chin. Phys. B . 2015, 24(12): 126201 . **doi:** 10.1088/1674-1056/24/12/126201

Effects of Cu on the martensitic transformation and magnetic properties of $Mn_{50}Ni_{40}In_{10}$ alloy

Li Ge-Tian, Liu Zhu-Hong, Meng Fan-Yan, Ma Xing-Qiao, Wu Guang-Heng
Chin. Phys. B . 2013, 22(12): 126201 . **doi:** 10.1088/1674-1056/22/12/126201

Static strength of gold compressed up to 127 GPa

Jing Qiu-Min, Wu Qiang, Liu Lei, Bi Yan, Zhang Yi, Liu Sheng-Gang, Xu Ji-An
Chin. Phys. B . 2012, 21(10): 106201 . **doi:** 10.1088/1674-1056/21/10/106201

Effect of chemical ordering annealing on superelasticity of Ni–Mn–Ga–Fe ferromagnetic shape memory alloy microwires*

Yanfen Liu(刘艳芬)[1,†], Xuexi Zhang(张学习)[2], Hongxian Shen(沈红先)[2], Jianfei Sun(孙剑飞)[2], Qinan Li(李奇楠)[1], Xiaohua Liu(刘晓华)[1], Jianjun Li(李建军)[1], and Weidong Cheng(程伟东)[1]

[1] *Department of Physics, Qiqihar University, Qiqihar* 161006, *China*
[2] *School of Materials Science and Engineering, Harbin Institute of Technology, Harbin* 150001, *China*

(Received 6 February 2020; accepted manuscript online 23 March 2020)

$Ni_{50}Mn_{25}Ga_{20}Fe_5$ ferromagnetic shape memory alloy microwires with diameters of ∼ 30–50 μm and grain sizes of ∼ 2–5 μm were prepared by melt-extraction technique. A step-wise chemical ordering annealing was carried out to improve the superelasticity strain and recovery ratio which were hampered by the internal stress, compositional inhomogeneity, and high-density defects in the as-extracted $Ni_{50}Mn_{25}Ga_{20}Fe_5$ microwires. The annealed microwires exhibited enhanced atomic ordering degree, narrow thermal hysteresis, and high saturation magnetization under a low magnetic field. As a result, the annealed microwire showed decreased superelastic critical stress, improved reversibility, and a high superelastic strain (1.9%) with a large recovery ratio (> 96%). This kind of filamentous material with superior superelastic effects may be promising materials for minor-devices.

Keywords: Ni–Mn–Ga–Fe microwire, chemical ordering annealing, martensite transformation, superelasticity

PACS: 62.20.fg, 71.20.Lp, 81.30.Kf **DOI:** 10.1088/1674-1056/ab8213

1. Introduction

Shape memory alloys (SMAs), such as Ni–Mn–Ga,[1] Ni–Ti,[2] Cu–Al–Ni,[3] and Fe–Pd[4] alloys, have attracted increasing attention in the past decade as promising candidate materials applicable in hydraulic, pneumatic, and motor-based systems. Ferromagnetic shape memory alloys (FMSMAs)[5] combine the martensite transformation and magnetic transitions and exhibit multi-functional properties, such as shape memory effect (SME),[1,6,7] superelasticity (SE),[8,9] magnetic-field-induced strain (MFIS),[10] and magnetocaloric effect (MCE)[11,12] driven by external thermal or magnetic fields. These excellent properties make FMSMAs potential candidate materials applying in sensors, actuators, and magnetic refrigerants (MR). SE in FMSMAs is also related to the stress-induced martensite (SIM) transformation when loading and reverse transformation upon unloading.[8] By taking advantages of the superelasticity, FMSMAs may be used for many products, e.g., cellular phone antennae, spectacle frames, medical guidewires and stents.[13]

Ni–Mn–Ga alloys have been widely studied in the past two decades. In order to improve the brittleness of Ni-Mn-Ga alloys, a fourth-element doping[14–20] and materials with fine grains[7,12,20–25] are the favorable methods. Recently, we reported the enhanced plastic deformation capability of Fe-doped $Ni_{49.7}Mn_{25.0}Ga_{19.8}Fe_{5.5}$ microwires due to the fine grains resulting from the melt-extraction process.[7,12,23,24] Further studies revealed the effect of the Fe content on the martensite transformation and superelasticity behaviors in the as-extracted $Ni_{50}Mn_{25}Ga_{25-x}Fe_x$ microwires.[24] Although the as-extracted microwires exhibited a superelastic strain > 0.75%, the recovery ratio was low due to the high defect density and internal stress induced by rapid quenching during melt-extraction. In addition, various magnetic coupled states were created in Ni–Mn–Ga microwires by varying the Fe-doping contents.[25] The magnitude of the direct magnetocaloric effect (DMCE) and inverse magnetocaloric effect (IMCE) could be feasibly adjusted by changing the Fe-doping contents.[25] This kind of filamentous material with both shape memory effect, superelasticity, and magnetocaloric properties has more broad application prospects.

As previously reported, an enhancement of magnetization and a reduction of MT hysteresis were observed in Ni–Mn–Ga microwires after annealing at 800 ℃. The improved MT and magnetic characteristics are related to the improvement of the antiferromagnetic Mn–Mn exchange interactions associated with reduction in the density of defects (such as vacancies, atomic disorders, and antiphase boundaries).[26] Our previous results also showed that, in $Ni_{50.6}Mn_{28}Ga_{21.4}$ alloy microwires, the defects and internal-stress could be reduced by annealing, which increased the elastic strain storage en-

*Project supported by the National Natural Science Foundation of China (Grant Nos. 51701099, 51801044, and 51671071), the Natural Science Foundation of Heilongjiang Province of China (Grant No. LH2019E091), and Fundamental Research Funds in Heilongjiang Provincial Universities, China (Grant No. 135409320). Thanks to the help of Technology Innovation Center of Agricultural Multi-Dimensional Sensor Information Perception, Heilongjiang Province.

†Corresponding author. E-mail: lxylyf_0@163.com

© 2020 Chinese Physical Society and IOP Publishing Ltd

ergy and reduced the energy dissipation.[27] As a result, the superelastic performance may be enhanced. Here, the as-extracted $Ni_{49.7}Mn_{25}Ga_{19.8}Fe_{5.5}$ microwires were subjected to a step-wise chemical ordering annealing heat treatment. The microstructure, martensite transformation, magnetic property, and superelasticity were investigated systematically. The results showed that the annealed microwires exhibited enhanced atomic ordering degree, narrow thermal hysteresis, and high saturation magnetization under a low magnetic field, which contributed to the high superelastic strain and large recovery ratio.

2. Experiment

Ni–Mn–Ga–Fe ingots were prepared by arc melting using pure elemental materials Ni (99.99%), Mn (99.99%), Ga (99.99%), and Fe (99.99%) in a high-purity argon atmosphere, followed by vacuum casting in a copper mold. The microwires with a nominal composition of $Ni_{49.7}Mn_{25}Ga_{19.8}Fe_{5.5}$ (atomic percent) were prepared by a melt-extraction technique using a copper wheel. Details of the fabrication process can be found in Ref. [24]. The as-extracted microwires were then subjected to a step-wise annealing heat-treatment allowing for chemical ordering. The annealing process was carried out at 993 K for 2 h, 953 K for 10 h, and 723 K for 20 h respectively, followed by furnace-cooling to room-temperature.

The grain morphology of the microwires was observed in a field-emission scanning electron microscopy (SEM-Helios Nanolab600i). The martensite twin structure was investigated using thin-foil specimens in a transmission electron microscope (Tecnai G^2 F30 TEM). The crystal structure of the as-extracted and annealed microwires was determined using a Philips X′Pert Pro instrument with Cu-K_α radiation (λ = 1.54 Å). The martensite and magnetic transition temperatures of the microwires were examined on a commercial magnetic property measurement system (MPMS) from Quantum Design. The measurement was carried out under a magnetic field of 10 Oe, by heating the microwires from 250 K to 400 K at 5 K/min, maintaining at 400 K for 5 min, and finally cooling to 250 K at 5 K/min. In order to remove the demagnetization effect, the microwires with aspect ratio > 30 were oriented parallel to the applied magnetic field. The superelastic test temperatures of a single microwire were determined from the internal friction ($\tan\delta$) versus temperature (T) curves on a dynamic mechanical analyzer (Q800 DMA), with oscillation frequency 1 Hz, strain amplitude 5×10^{-4}, and heating/cooling rates 5 K/min. The optimized superelastic test temperatures were determined to be $\sim$ 310 K and $\sim$ 318 K (higher than M_s) for the as-extracted and annealed microwires, respectively. The loading and unloading rates were 0.04 N/min during the superelastic tests.

3. Results and discussion

3.1. Effect of chemical ordering annealing on microstructure

During the melt-extraction process, the melt filaments are subjected to an extremely high solidification rate, leading to the formation of fine grains (grain size of $\sim$ 1 μm, as illustrated in Fig. 1(a)). In Fig. 1(b), the microwires exhibit diameters of $\sim$ 30–50 μm, with D-shaped cross-section. The cross-section consists of a plane part, formed by contact of the molten alloy and the copper wheel; and a semicircular part, formed by free solidification of the melt.[7,12,20,21,23,24] After annealing, the grain grows and the grain size increases as shown in Fig. 1(c). The fan-shaped oriented columnar grains are 1–2 μm and 2–5 μm in width in the as-extracted and annealed microwires (see Figs. 1(b) and 1(d)), respectively. Furthermore, the defect density and internal stress formed by rapid solidification are reduced by annealing.[27]

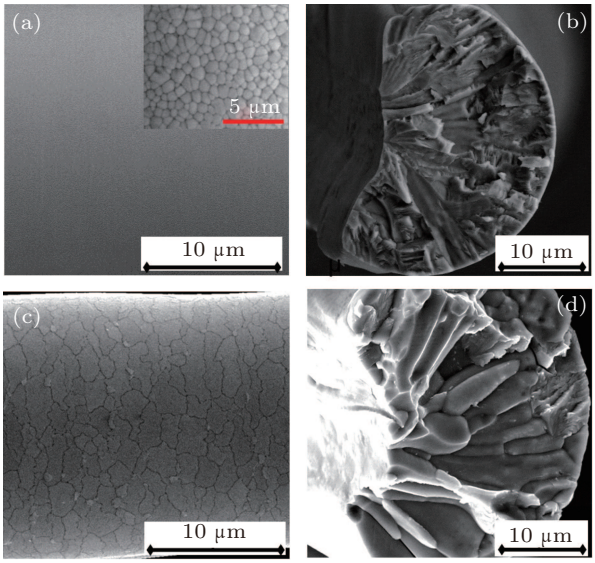


Fig. 1. SEM micrographs of the grains and fracture surfaces of the $Ni_{50}Mn_{25}Ga_{20}Fe_5$ microwires: (a), (b) the as-extracted microwires, and (c), (d) the annealed microwires.

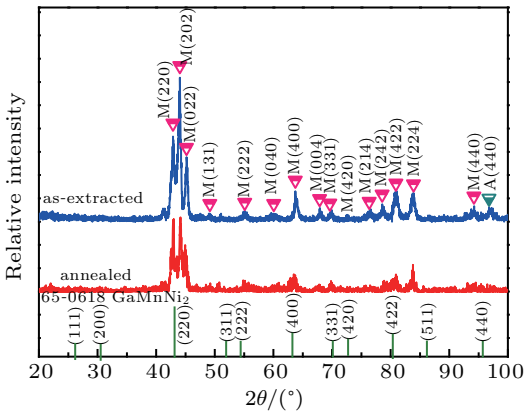


Fig. 2. XRD patterns of as-extracted and annealed $Ni_{50}Mn_{25}Ga_{20}Fe_5$ microwires.

Figure 2 displays the x-ray diffraction (XRD) patterns of the as-extracted and annealed microwires which are measured

at room temperature. The as-extracted microwires consist of the martensite and austenite phases, while the annealed microwires contain only the martensite phase. The reflections are indexed on an orthorhombic structure.

The martensite twin structures in the extracted and annealed microwires are further investigated by TEM as displayed in Fig. 3. At the temperature of 25 ℃, the bright field images in Figs. 3(a) and 3(b) show that the stripe-like martensite twins variants A and B (or C and D) exhibit a self-accommodated morphology. Compared with the as-extracted microwire, the density of dislocation is significantly reduced after annealing. In the annealed microwire, the martensite twin boundaries are straighter and clearer than those in the as-extracted one. This implies the enhancement in the atomic ordering degree and the reduction in the defect density after annealing. The diffraction patterns of the martensite twins are shown in the insets of Figs. 3(a) and 3(b). The electron diffraction pattern in the inset of Fig. 3(a) displays the modulation structure of the as-extracted microwires (six periodically spots distribute between two main spots), showing that both extracted and annealed microwires exhibit a seven-layered modulated (7M) martensite structure with crystal lattice parameters of $a = 6.123$ Å, $b = 5.804$ Å, $c = 5.546$ Å and $a = 6.095$ Å, $b = 5.812$ Å, $c = 5.564$ Å before and after annealing, respectively. The 7M martensite has a lower free energy and it is more stable performing the reverse martensitic transformation.[28] This may be related to the high internal stress formed during the rapid solidification process, which favors the formation of 7M martensite.[27]

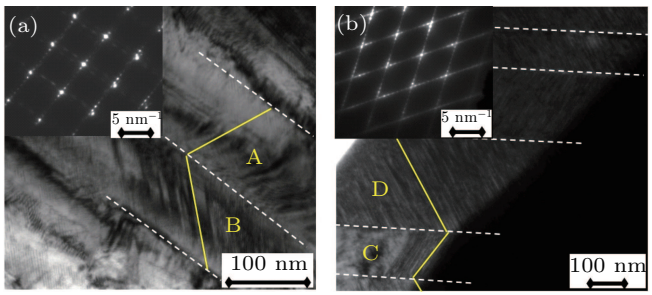


Fig. 3. TEM micrographs of martensite twin structure for (a) as-extracted and (b) annealed $Ni_{50}Mn_{25}Ga_{20}Fe_5$ microwires. Insets in (a) and (b) are the corresponding diffraction patterns of the martensite phase showing 7M modulated structure, respectively.

3.2. Martensite transformation after chemical ordering annealing

The temperature dependence of magnetization (M–T) curves of the microwires are shown in Fig. 4(a). During the heating process, both microwires show martensite to austenite reverse transformation followed by the magnetic transition of the austenite phase. The abrupt change of magnetization during the cooling process corresponds to a parent austenite to martensite transformation. The martensite and austenite starting and finishing transformation temperatures (denoted by M_s, M_f, A_s, and A_f) are 305 K, 292 K, 301 K, and 312 K, respectively, for the as-extracted microwire. On the other hand, the annealed microwire has M_s, M_f, A_s, and A_f of 327 K, 302 K, 308 K, and 328 K, respectively, which are slightly higher than those of the extracted microwire. The phase transition data of the as-extracted and annealed $Ni_{50}Mn_{25}Ga_{20}Fe_5$ microwires obtained from the M–T and M–H curves are listed in Table 1. The thermal hysteresis ($\Delta T = A_f - M_s$) is determined to be 7 K and 1 K for the as-extracted and annealed microwires, respectively. Thus, the thermal hysteresis significantly decreases after annealing. After the annealing treatment, both frictional work and stored elastic strain energy dissipation are reduced due to the decreased internal stresses and defects density.[29] The effect of annealing on M–T and thermal hysteresis of the microwires is related to the compositional homogeneity, Ga vacancy concentration, long-range atomic ordering, and elimination of internal stress and defects.[27] The increase of the martensite transformation temperature may be attributed to the reduction in the defect density and internal stress.[19] In addition, the electron concentration (e/a) increases when Fe ($3d^6 4s^2$) replaces Ga ($4s^2 4p^1$), which also leads to the increase of the martensite transformation temperature.

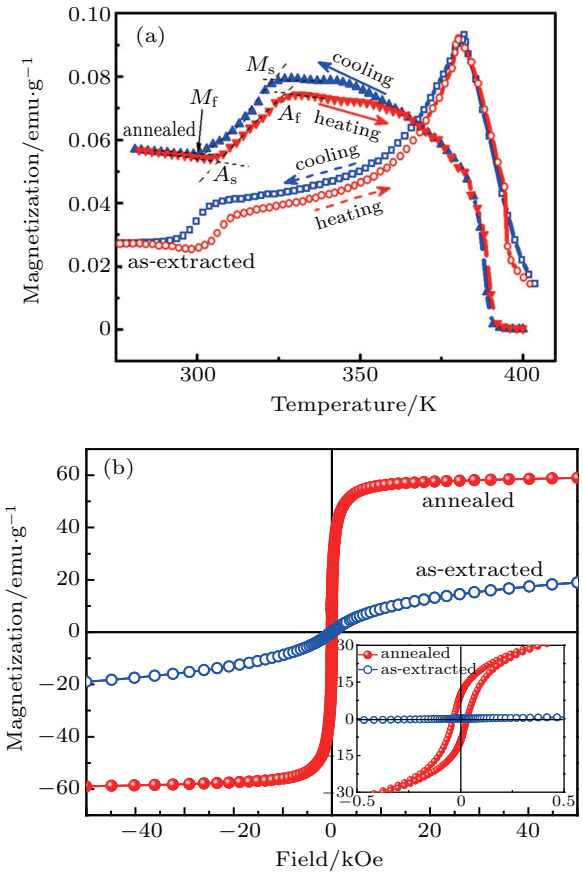


Fig. 4. Magnetic properties of as-extracted and annealed $Ni_{50}Mn_{25}Ga_{20}Fe_5$ microwires. (a) Magnetization vs. temperature (M–T) curves under an external magnetic field of 10 Oe. (b) Magnetization curves (M–H) at room temperature.

Figure 4(b) shows the hysteresis loops of the as-extracted and annealed microwires at room-temperature. The as-

extracted microwire shows ferrimagnetism while the annealed one ferromagnetism. As shown in the inset of Fig. 4(b), the magnetization curves of the as-extracted and annealed microwires show a slope change with increasing field. The annealed microwire saturates under a low magnetic field of 15 kOe and also displays a higher saturation magnetization increased from 20 emu/g to 60 emu/g compared with the as-extracted microwire. This indicates that the magnetic anisotropy after chemical annealing is higher than that at the as-extracted state.[23,27] This also results from the compositional homogenization of chemical ordering annealing.[19,25] The coercivity of the annealed microwires is only ~ 36 Oe, as shown in the inset of Fig. 4(b). Since the magnetism in Ni–Mn–Ga alloys is thought to be mainly due to the Mn–Mn atomic interaction, the increase of the saturation field can be addressed to Mn atoms ordering in the lattice.[23,27] The hysteresis loss of the annealed microwire is also very small, which is considered beneficial to the magnetocaloric effect.[12]

Table 1. Phase transition data of the as-extracted and annealed $Ni_{50}Mn_{25}Ga_{20}Fe_5$ microwires obtained from M–T and M–H curves.

Material state	Martensite transformation temperature/K					Curie temperature/K	Saturation field/Oe	Magnetization/emu·g^{-1}
	M_s	M_f	A_s	A_f	ΔT			
As-extracted	305	292	301	312	7	394	–	unsaturation
Annealed	327	302	308	328	1	390	15	60

3.3. Superelasticity after chemical ordering annealing

To determine the superelastic test temperature of a microwire, tanδ–T curves are measured for an annealed microwire as shown in Fig. 5. The annealed wire has tan$\delta = 0.02$ in its austenite state, which is increased to a peak value 0.23 at 310 K during the cooling process, corresponding to the parent to martensite phase transformation. The tanδ of the martensite is ~ 0.04, slightly higher than that of the austenite phase. During the heating process, tanδ drops from ~ 0.04 of the martensite to ~ 0.02 of the austenite state after the reverse martensite transformation with peak temperature centered at 336 K. On the other hand, the tanδ peaks correspond to a dip of the elastic storage modulus (right hand side of Fig. 5), indicating the lattice vibration softening during the austenite $\rightarrow$ martensite transformation, which can be explained by the localized soft mode theory (LSMT).[24,30]

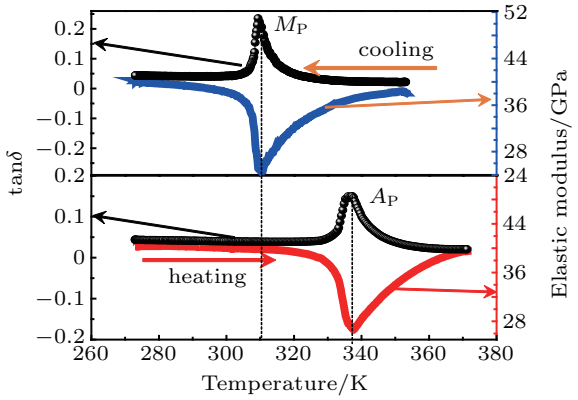


Fig. 5. Temperature dependent internal friction (tanδ–T) and storage modulus of annealed $Ni_{50}Mn_{25}Ga_{20}Fe_5$ microwire.

The superelastic tests of the as-extracted and annealed microwires are conducted at temperatures higher than their M_s. The tensile stress–strain curves under different loadings for the as-extracted and annealed microwires at temperatures 310 K and 318 K are displayed in Figs. 6(a) and 6(b), respectively. The experimental data of the as-extracted and annealed $Ni_{50}Mn_{25}Ga_{20}Fe_5$ microwires obtained from the tensile stress–strain curves are listed in Table 2. The as-extracted microwire is loaded to 375 MPa for reaching a strain of ε_t, then it is unloaded to zero stress leaving a residual strain ε_r. The recoverable strain consists of elastic strain ε_e and SE strain ε_{SE} ($\varepsilon_{SE} = \varepsilon_t - \varepsilon_e - \varepsilon_r$).[24] The maximum stress-induced strains without breaking reach 1.5% at 310 K under 375 MPa for the as-extracted microwire and 2.0% at 318 K under 310 MPa for the annealed microwire. The elastic deformation of austenite occurs at an early stage, after which the stress-induced martensite transition (SIMT) happens, which results in the decrease of gradient in the superelastic plateau.[8] The microwires before and after annealing both possess the superelastic effect. Upon unloading, the strain partly recovers, either by elastic deformation or incomplete martensite to austenite transition, suggesting the occurrence of stress-induced austenite transition (SIAT). The selection of the SIM and SIA critical stresses is shown in Fig. 6(b). For both microwires, the stress–strain curves overlap during the loading process, demonstrating a well reproduction during the SIMT process. Under the same stress level, the strain achieved in the annealed microwire is much higher than that in the extracted microwire, revealing the low modulus and high mobility of the twin boundaries due to the enhancement in atomic ordering degree and reduction in defect density in the annealed microwire. The annealed microwire sustains a strain larger than 2.0% without fracture due to the high specific free surface area (SSA) and size effect. Upon unloading, the strain partly recovers in the as-extracted microwires, but completely recovers in the annealed one. As the residual strain is unfavorable for the reversibility, the annealed microwires show enhanced superelastic property compared to the as-extracted ones. And the SE strain of the an-

nealed microwire is up to 1.9%. The critical SIA stresses are reduced after annealing because annealing can enhance the atomic ordering degree, improve the composition homogeneity, and reduce both defect density and internal stress, which all favor the shear deformation process and are consistent with the TEM graphs in Fig. 3.

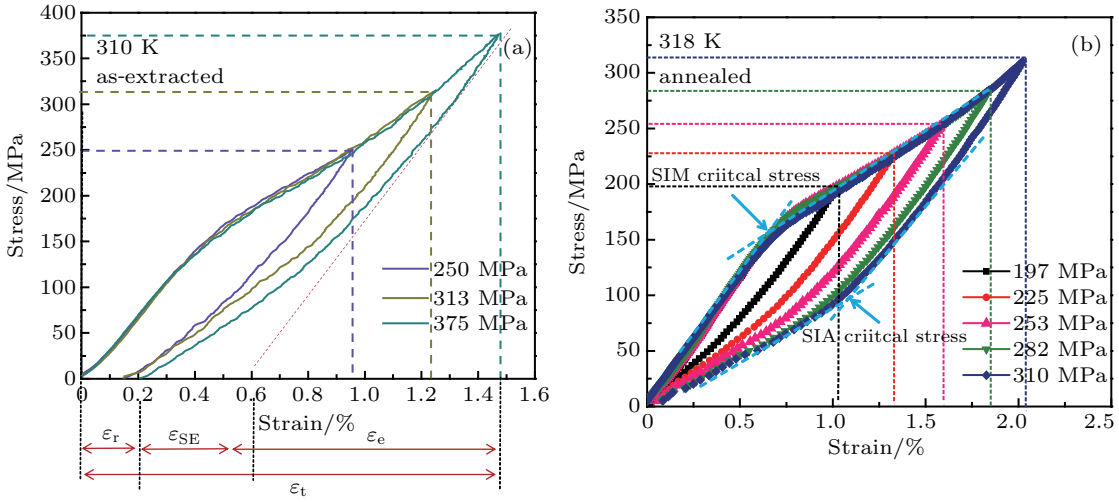


Fig. 6. Tensile stress–strain curves under different loadings for (a) as-extracted $Ni_{50}Mn_{25}Ga_{20}Fe_5$ microwires at temperature of 310 K and (b) annealed ones at temperature of 318 K.

Table 2. Experimental data of the as-extracted and annealed $Ni_{50}Mn_{25}Ga_{20}Fe_5$ microwires obtained from tensile stress–strain curves.

Material state	Stress loadings/MPa	Total stain/%	SE strain/%	Recovery ratio/%	SIM critical stress/MPa	SIA critical stress/MPa
As-extracted	250	1.0	0.3	85.2	152	128
	313	1.2	0.4	85.5	150	154
	375	1.5	0.4	86.0	156	146
Annealed	197	1.0	0.2	94.5	170	104
	225	1.3	1.3	96.2	165	101
	253	1.6	1.5	96.5	165	102
	282	1.8	1.7	96.0	167	104
	310	2.0	1.9	96.5	157	108

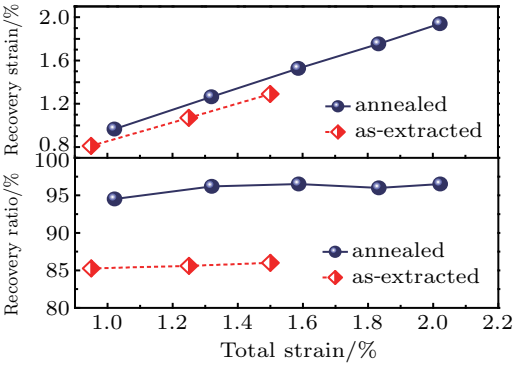


Fig. 7. Recovery strain and recovery ratio under various total strains for the as-extracted and annealed $Ni_{50}Mn_{25}Ga_{20}Fe_5$ microwires.

The reversibility of superelasticity is also important for the practical application of SMAs. Figure 7 shows the recovery ratio and recovery strain in the as-extracted and annealed microwires. For comparison, the calculation is carried out with the same total strain for both microwires. The annealed microwires have superior recovery strain and recovery ratio ($> 96\%$), meaning almost completely recovery of the plastic deformation strain. The recovery ratio of the as-extracted microwire is $\sim 85\%$, which results from the internal stress restricting the formation of self-accommodate martensite variants.[7,24] As a result, higher elastic strain energy accumulates in the as-extracted microwire, which acts as resistance to the forward transformation. In addition, the increase of the atomic ordering degree makes shear transformation easier,[31] less defects and composition homogenization after annealing increase the mobility of the martensite twin boundaries, which also favors the SIM process.[27] The above results show that the annealed microwires are superior for practical applications.

4. Conclusions

The effects of step-wise chemical ordering annealing on the microstructure, martensite transformation, and superelasticity in polycrystalline $Ni_{50}Mn_{25}Ga_{20}Fe_5$ microwires were investigated. The annealed microwires exhibited narrow thermal hysteresis, lower saturated magnetization field, higher superelastic strain, higher recovery ratio, higher magnetization, and a near room temperature MT compared with the as-cast wires. Given these properties, these microwires can be used

as candidate materials in various micro-devices and micro-sensor. The main conclusions can be drawn as follows.

(1) After chemical ordering annealing, with the increase in the atomic ordering as well as the decrease in the internal stress and defect density, the microwires showed seven-layered modulated structure and straight martensite variant twin boundaries, with each variant forming an adaptive configuration and showing good consistency.

(2) Chemical ordering annealing promoted the transition temperature by ~ 20 K and decreased the thermal hysteresis by ~ 6 K for the microwire, this may be attributed to the reduction in the defect density and internal stress. The annealed microwires exhibited a saturation magnetization of ~ 60 emu/g under a low magnetic field of ~ 15 kOe, the increase of the saturation field can be attributed to Mn atoms ordering in the lattice.

(3) The superelasticity may also be tailored by the chemical ordering annealing: the SIA stress was reduced and the reversibility during superelastic cycles was improved. The annealed microwire showed SE strain of $\sim 1.9\%$ and a higher recovery ratio of strain $> 96\%$.

References

[1] Webster P J, Ziebeck K R A, Town S L and Peak M S 1984 *Philos Mag. B* **49** 295
[2] Zhou M, Li Y S, Zhang C and Li L F 2018 *Chin. Phys. B* **27** 106501
[3] Gómez-Cortés J F, Nó M L, López-Echarri A, Ruiz-Larrea I, Breczewski T and San J 2018 *Phys. Stat. Sol. A* **215** 1800340
[4] Xiao F, Chu K J, Jin X J, Ren F Z, Fukuda T, Kakeshita T and Sun Q P 2018 *Scr. Mater.* **152** 141
[5] Hassan N, Shah I A, Khan T, Liu J, Gong Y Y, Miao X F and Xu F 2018 *Chin. Phys. B* **27** 037504
[6] Xin Y and Li Y 2016 *Mater. Sci. Eng. A* **649** 254
[7] Liu Y F, Zhang X X, Xing D W, Qian M F, Shen H X, Wang H, Liu J S and Sun J F 2014 *Phys. Stat. Sol. A* **211** 2532
[8] Chernenko V A, Villa E, Salazar D and Barandiaran J M 2016 *Appl. Phys. Lett.* **108** 071903
[9] Wang Z L, Zheng P, Nie Z H, Ren Y, Wang Y D, Müllner P and Dunand D C 2015 *Acta Mater.* **99** 373
[10] Chmielus M, Zhang X X, Witherspoon C, Dunand D C and Müllner P 2009 *Nat. Mater.* **8** 863
[11] Shah I A, Hassan N, Rauf A, Liu J, Gong Y Y, Xu G Z and Xu F 2017 *Chin. Phys. B* **26** 097501
[12] Liu Y F, Zhang X X, Xing D W, Shen H X, Liu J S and Sun J F 2014 *J. Alloys Compd.* **616** 184
[13] Mas B, Biggs B, Vieito A, Cladera A, Shaw J and Martínez-Abella F 2017 *Constr. Build. Mater.* **148** 307
[14] Zhang X X, Qian M F, Wang G H, Xu P F, Geng L and Sun J F 2017 *Rare Met.* **137** 1
[15] Li P P, Wang J M and Jiang C B 2011 *Chin. Phys. B* **20** 028104
[16] Barabash R I, Barabash O M, Popov D, Shen G Y, Park C Y and Yang W G 2015 *Acta Mater.* **87** 344
[17] Tan C H, Jiang J X, Tian X H and Cai W 2010 *Chin. Phys. B* **19** 107102
[18] Pérez-Checa A, Feuchtwanger J, Barandiaran J M, Sozinov A, Ullakko K and Chernenko V A 2018 *Scr. Mater.* **154** 131
[19] Diestel A, Niemann R, Schleicher B, Schwabe S, Schultz L and Fähler S 2015 *J. Appl. Phys.* **118** 023908
[20] Zhang X X, Qian M F, Zhang Z, Wei L S, Geng L and Sun J F 2016 *Appl. Phys. Lett.* **108** 052401
[21] Qian M F, Zhang X X, Wei L S, Martin P G, Sun J F, Geng L, Scott T B, Panina L V and Peng H X 2016 *J. Alloys Compd.* **660** 244
[22] Lin Z B, Zhang Y D, Sanchez-valdes C F, Sanchez J L, Esling C, Zhao X and Zuo L 2014 *Appl. Phys. Lett.* **104** 044101
[23] Liu Y F, Zhang X X, Xing D W, Qian M F, Shen H X, Wang H, Liu J S and Sun J F 2015 *Phys. Stat. Sol. A* **212** 855
[24] Liu Y F, Zhang X X, Xing D W, Shen H X, Qian M F, Liu J S, Chen D M and Sun J F 2015 *Mater. Sci. Eng. A* **636** 157
[25] Liu Y F, Luo L, Zhang X X, Shen H X, Liu J S, Sun J F and Zu N N 2019 *Intermetallics* **112** 106538
[26] Gómez-Polo C, Pérez-Landazábal J I, Recarte V, Sánchez-Alarcos V, Badini G C and Vázquez M 2010 *J. Appl. Phys.* **107** 123908
[27] Qian M F, Zhang X X, Wei L S, Geng L and Peng H X 2015 *J. Alloys Compd.* **645** 335
[28] Jiang C B, Muhammad Y, Deng L F, Wu W and Xu H B 2004 *Acta Mater.* **52** 2779
[29] Kokorin V V, Kozlova L E and Titenko A N 2002 *Scr. Mater.* **47** 499
[30] Guénin G and Gobin P F 1982 *Metall. Trans. A* **13** 1127
[31] Cui Y T, Wu L, You S Q, Zhang J, Wu Z X, Kong C Y, Chen J L and Wu G H 2009 *Solid State Commun.* **149** 1539